Available online at www.sciencedirect.com
SCIENCE DIRECT®
Sensors and Actuators A 106 (2003) 187–194
SENSORS AND ACTUATORS A PHYSICAL
www.elsevier.com/locate/sna

GMI modeling and material optimization

Luděk Kraus*
Institute of Physics, Academy of Sciences of the Czech Republic, Prague, Czech Republic

Abstract

A review of theoretical models of giant magnetoimpedance (GMI) is presented. The whole frequency range from kHz to GHz is covered starting from the simple quasistatic models and ending with the complex dynamic models based on the simultaneous solution of linearized Maxwell and Landau–Lifshitz equations. The similarity between GMI and FMR is emphasized. The asymmetric GMI (AGMI) behavior is discussed in more detail. Three different mechanisms of asymmetry are outlined. Based on the theoretical results the rules for obtaining high performance GMI materials are put forward.

Keywords: Magnetic field sensors; Giant magnetoimpedance; Soft magnetic materials

1. Introduction

The giant magnetoimpedance (GMI), the huge change of ac impedance of soft magnetic conductors upon application of dc magnetic field, attracts much attention of research teams all over the world because of its perspective applications. The GMI-based devices are already achieving a development stage that is mature enough to enter in the relevant area of extremely sensitive magnetic field and strain sensors. The design of new application oriented materials, however, requires a deeper understanding of magnetic structure and magnetization dynamics of soft magnetic metals. The aim of this paper is to make a brief review of theoretical models of GMI and to show how they can be used to optimize the properties of GMI materials for sensing applications.

According to definition, the complex impedance, $Z(\omega) = R + \mathrm{i}X$, is given by the ratio $U_{\mathrm{ac}}/I_{\mathrm{ac}}$, where I_{ac} is the amplitude of sinusoidal current passing through the conductor and U_{ac} the voltage measured between its ends. In ferromagnetic metals this definition has only limited validity, because a ferromagnetic metal is generally a non-linear material. In linear approximation, the GMI ratio is:

$$\frac{Z}{R_{\mathrm{dc}}} = \frac{j_z(S)}{\langle j_z \rangle_q} \tag{1}$$

where R_{dc} is the dc resistance, $j_z(S)$ the axial component of current density on the surface and $\langle j_z \rangle_q$ is its average value over the conductor cross-section q. Alternatively, the ratio can be obtained from the surface impedance tensor $\hat{\zeta}$:

$$\frac{Z}{R_{\mathrm{dc}}} = \frac{q}{\rho l}\left(\zeta_{zz} - \zeta_{z\phi}\frac{h_z(S)}{h_\phi(S)}\right) \tag{2}$$

where ρ is the resistivity, l the length of cross-section contour and h_z and h_ϕ are the axial and circumferential components of ac magnetic field, respectively.

The current density $\boldsymbol{j}$ or the magnetic field $\boldsymbol{h}$ can be obtained, within the frame of classical electrodynamics of continuous media, by the simultaneous solution Maxwell equations and Landau–Lifshitz equation of motion. For low-signal approximation, the following linearized equations are obtained:

$$\nabla^2 \boldsymbol{h} - \frac{2\mathrm{i}}{\delta_0^2}\boldsymbol{h} = \frac{2\mathrm{i}}{\delta_0^2}\boldsymbol{m} - \mathrm{grad}\,\mathrm{div}\,\boldsymbol{m} \tag{3}$$

where $\delta_0 = \sqrt{2\rho/\omega\mu_0}$ is the non-magnetic skin depth and $\boldsymbol{m}$ is the ac component of magnetization, and

$$\mathrm{i}\frac{\omega}{\gamma}\boldsymbol{m} = \boldsymbol{m} \times \left(\boldsymbol{H}_{\mathrm{eff},0} + \mathrm{i}\frac{\alpha\omega}{\gamma M_{\mathrm{s}}}\boldsymbol{M}_0\right) + \boldsymbol{M}_0 \times \boldsymbol{h}_{\mathrm{eff}} \tag{4}$$

where $\boldsymbol{M}_0$ and $\boldsymbol{H}_{\mathrm{eff},0}$ are the equilibrium dc components of magnetization and effective field, respectively, $\boldsymbol{h}_{\mathrm{eff}}$ the ac component of effective field, γ the gyromagnetic ratio and α is the Gilbert damping parameter. Different theoretical models use different simplifying assumptions to get the approximate solution of Eqs. (3) and (4) with appropriate boundary conditions.

Using the simple material relation $\boldsymbol{m} = \chi\boldsymbol{h}$, instead of Eq. (4), the well known classical skin effect solution of

* Tel.: +420-2-6605-2174; fax: +420-2-8689-0527.
E-mail address: kraus@fzu.cz (L. Kraus).

0924-4247/$ – see front matter © 2003 Elsevier B.V. All rights reserved.
doi:10.1016/S0924-4247(03)00164-X

Eq. (3) can be found [1]. For example for a cylindrical wire with the radius a:

$$\frac{Z}{R_{dc}} = ka\frac{J_0(ka)}{2J_1(ka)} \tag{5}$$

and for an infinite film of thickness t are obtained.

$$\frac{Z}{R_{dc}} = k\frac{t}{2}\cot\left(k\frac{t}{2}\right) \tag{6}$$

Here, the propagation constant k is given by $k = (1 - i)/\delta$, with the classical skin depth $\delta = \sqrt{2\rho/\omega\mu_0(1 + \chi)}$.

2. Theoretical models

Depending on the frequency ω of the driving current I_{ac} the giant magnetoimpedance can be roughly separated into four frequency regimes:

(i) *Very low frequencies*, from zero up to about 10 kHz. Large voltage peaks between the sample ends are induced mainly due to large Barkhausen jumps in the circular magnetization [2]. The behaviour is highly non-linear. The skin effect is very weak and mainly the reactance X contributes to the impedance change. For low-signal levels, where the sample could exhibit nearly linear behaviour, the effect is very weak and hardly observable.

(ii) *Low frequencies*, from about 10 kHz to about 1 MHz. GMI originates basically from the variations of the skin depth due to strong changes of the effective magnetic permeability caused by a static magnetic field. In this case, both domain walls and magnetization rotation contribute to the circumferential permeability.

(iii) *Intermediate frequencies*, from about 1 MHz to few hundred MHz. In this regime, the domain walls are already strongly damped by eddy currents and only magnetization rotation contributes to GMI.

(iv) *Very high frequencies*, of the order of GHz. The magnetization rotation is strongly influenced by the gyromagnetic effect and the ferromagnetic relaxation. The impedance maxima are shifted to higher fields, where samples are already magnetically saturated. Strong changes in magnetic penetration depth are caused by the same mechanisms as in the ferromagnetic resonance.

The theoretical models can be divided into three categories, which are closely related to the frequency ranges discussed above.

2.1. Quasistatic models

These models are based on the assumption that the frequency is so small that an equilibrium state of the system can be reached at every moment. Then Eqs. (5) and (6) can be used with the effective circumferential susceptibility χ calculated from Eq. (4), where $\omega = 0$. This procedure is equivalent to the minimization of free energy.

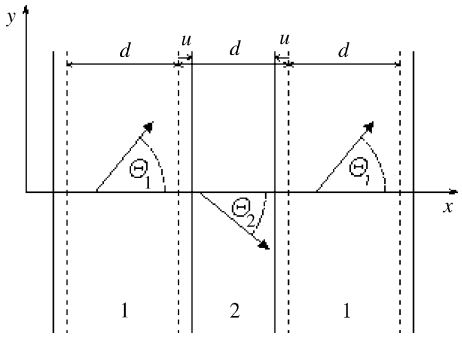

Fig. 1. Domain structure of a uniaxial film with the easy direction along y-axis.

Machado and Rezende [3] and Atkinson and Squire [4] investigated GMI in a film with an in-plane anisotropy and periodic domain structure as shown in Fig. 1. The transversal susceptibility was obtained by minimizing the free energy with respect to the parameters θ_1, θ_2 and u.

If the easy direction is perpendicular to the conductor axis (then $\boldsymbol{H}_0 || x$ and $\boldsymbol{h} || y$) both, domain wall movement and magnetization rotation, contribute to the circumferential susceptibility. If the domain wall displacement dominates and the magnetization rotation is neglected then $\cos\theta_1 = \cos\theta_2 = \cos\theta_0 = H_0/H_K$ and the transverse susceptibility due to domain wall movement is:

$$\chi_{t,dw} = \frac{2u}{dh}M_s\sin\theta_0 = \frac{4\mu_0 M_s^2}{\beta}\left(1 - \frac{H_0^2}{H_K^2}\right) \tag{7}$$

where β is the wall pinning parameter and H_K the anisotropy field. The field dependence of $\chi_{t,dw}$ is shown in Fig. 2 (curve a). On the other hand, if the walls are completely pinned

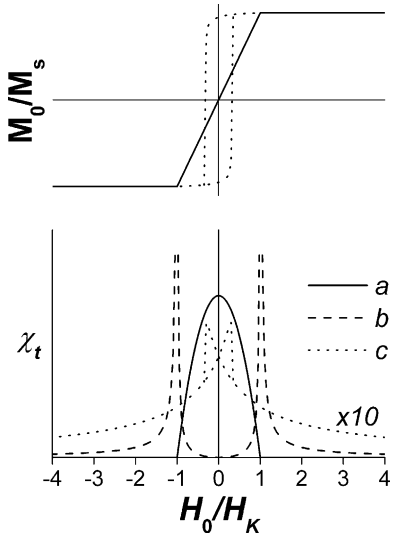

Fig. 2. Transverse susceptibility calculated for a uniaxial film: (a) $\boldsymbol{H}_0 \perp$ easy axis: domain wall movement, (b) $\boldsymbol{H}_0 \perp$ easy axis: magnetization rotation, (c) $\boldsymbol{H}_0 \parallel$ easy axis.

($u = 0$), the transverse susceptibility $\chi_{t,rot}$ calculated from Eq. (4) is then (see, for example [5]):

$$\chi_{t,rot} = \frac{M_s \cos^2 \theta_0}{H_0 \cos \theta_0 - H_K \cos 2\theta_0} \quad (8)$$

The field dependence of rotational susceptibility (curve b in Fig. 2) exhibits singularities at $H_0 = \pm H_K$, where the torque of anisotropy exerted by the magnetic moment is compensated by the dc field and a free rotation of magnetization is allowed. In real materials, the sharp peaks are smeared out by the damping of magnetization motion and by the dispersion of local anisotropies [4,5].

If the easy direction is parallel to the conductor axis (then $\boldsymbol{H}_0 || y$ and $\boldsymbol{h} || x$), the domain walls do not contribute to GMI and the transverse susceptibility is:

$$\chi_{t,rot} = \frac{M_s}{H_K} \frac{(1 - (M_0/M_s)(H_0/H_K))}{(1 - (H_0^2/H_K^2))} \quad (9)$$

where $M_0 = 2M_s u/d$ is the total dc magnetization. The field dependence of transverse susceptibility, calculated for the hysteresis loop $M_0(H_0)$ shown in the upper part of Fig. 2 (dotted line), is shown by the curve c.

Though the quasistatic models cannot explain the frequency dependence and other GMI properties, they can well describe some basic features of GMI not only in films but also in ribbons and wires.

2.2. Eddy current damping of domain wall movement

Generally, both the domain wall movement and the magnetization rotation contribute to the total circumferential susceptibility:

$$\chi_t = \chi_{t,dw} + \chi_{t,rot} \quad (10)$$

In metallic ferromagnets the domain wall movements are heavily damped. At medium frequencies, the quasistatic model can be used only if the eddy current damping of domain walls is properly taken into account.

The rough estimate of the influence of driving current frequency on GMI can be obtained by varying the domain wall pinning parameter β in Eq. (7). It was shown that with increasing β the continuous change from single- to double-peak behavior takes place for the case of transversal anisotropy [4]. Machado and Rezende [3] used a viscous friction force to describe phenomenologically the damping of domain wall motion. Then the frequency dependence of transversal susceptibility is given by

$$\chi_{t,dw} = \frac{\chi_0}{1 - i\tau\omega} \quad (11)$$

where the phenomenological relaxation time τ is the fitting parameter. More rigorous treatment can be found in [6], where the effective medium approximation was used for the calculation of circumferential permeability for a periodic bamboo-like domain structure in cylindrical wires. The same formula as Eq. (11) was obtained with the relaxation time $\tau = b\chi_0/\rho$, where the proportionality constant b depends only on the wire diameter and the domain structure period. Exact solution of eddy current problem in a cylindrical wire with periodic bamboo-like domain structure was done by Chen et al. [7].

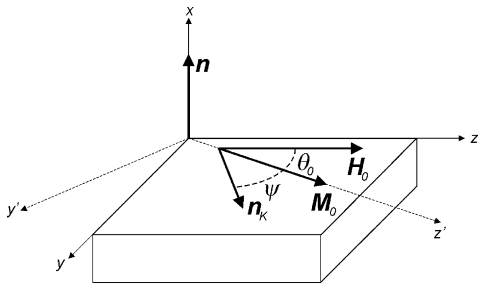

Fig. 3. Coordinate systems in a single-domain planar film.

2.3. High frequency models of GMI

It has been proved, both theoretically and experimentally, that the domain wall motion in typical soft magnetic metals practically stops in the frequency region of few 10ths to few MHz. Therefore, at high frequencies the domain walls contribution to GMI effect can be neglected and only the magnetization rotations can be considered. There the procedures known from the theory of ferromagnetic resonance are suitable for the solution of Eqs. (3) and (4). In the following, the high frequency models will be divided into two categories according to whether they take into account the exchange interaction in the effective field $\boldsymbol{H}_{eff}$ or not.

2.3.1. Electromagnetic models

When the exchange interaction is neglected, the linearized Landau–Lifshitz Eq. (4) represents a linear relation $\boldsymbol{m} = \hat{\chi}(\boldsymbol{r})\boldsymbol{h}$ between the ac components of magnetization and magnetic field, where $\hat{\chi}(\boldsymbol{r})$ is the local susceptibility tensor. Using this relation in Eq. (3), a partial differential equation for $\boldsymbol{h}$ is obtained. In real materials $\hat{\chi}(\boldsymbol{r})$ may be a complex function of coordinates, which makes the modeling very difficult. To simplify the solution, simple magnetic structures, free of magnetic domains, and simple geometrical shapes (circular cylinders or infinite planar films) were investigated.

An example of the electromagnetic models will be shown here. Let us assume an infinite single-domain planar film (Fig. 3) with an in-plane uniaxial anisotropy. All, the dc field $\boldsymbol{H}_0$, the static magnetization $\boldsymbol{M}_0$, and the unit vector $\boldsymbol{n}_K$ of the anisotropy easy axis lie in the film plane. Then the susceptibility tensor is constant in the sample volume. By the same procedure as in the FMR theory, the effective transverse susceptibility can be calculated [8]:

$$\chi_t = \frac{M_s \cos^2 \theta_0 (\Omega + M_s + H_K \cos^2 \psi)}{(\Omega + H_K \cos 2\psi)(\Omega + M_s + H_K \cos^2 \psi) - (\omega/\gamma)^2} \quad (12)$$

where

$$\Omega = H_0 \cos\theta_0 + \mathrm{i}\alpha\frac{\omega}{\gamma} \tag{13}$$

and the equilibrium angle θ_0 is given by the equation:

$$H_0 \sin\theta_0 - \tfrac{1}{2} H_\mathrm{K} \sin 2\psi = 0 \tag{14}$$

The field dependence of skin depth δ can be calculated from Eq. (12). Then the magnetoimpedance of a wire with helical anisotropy or a ribbon with in-plane anisotropy can be obtained using Eq. (5) or Eq. (6), respectively [5,8].

The close relation between GMI and FMR, which has been pointed out by Yelon et al. [9], can be demonstrated on Eq. (12). Transverse susceptibility χ_t shows the typical resonance behavior with the maximum of imaginary part χ_t'' and the change of sign of real part χ_t' at the resonance field determined by the FMR resonance condition:

$$\left(\frac{\omega}{\gamma}\right)^2 = (H_0 \cos\theta_0 + H_\mathrm{K} \cos 2\psi)(H_0 \cos\theta_0 + M_\mathrm{s} + H_\mathrm{K} \cos^2\psi) \tag{15}$$

Then the theoretical skin depth reaches its minimum value

$$\delta_\mathrm{m} = \sqrt{\frac{\alpha\rho}{\gamma\mu_0 M_\mathrm{s}}} \tag{16}$$

and the GMI ratio its maximum. The maximum theoretical $|Z|/R_\mathrm{dc}$ is frequency independent and its magnitude is, with the exception of GHz frequencies, much larger than is experimentally observed [10].

The resonance frequency versus applied field, calculated with material parameters typical for low magnetostrictive amorphous alloys, is shown in Fig. 4. As can be seen, for frequencies less then 100 MHz, where GMI is usually measured, the resonance condition cannot be easily satisfied. It is fulfilled for $H_0 \approx H_\mathrm{K}$, but only if the anisotropy axis is very precisely perpendicular to the dc field direction. Any small deviation or fluctuation of easy direction substantially reduces the GMI ratio at lower frequencies. With increasing frequency, these effects become less important and in the GHz region the experimentally observed GMI ratios well satisfy the theoretical prediction [11].

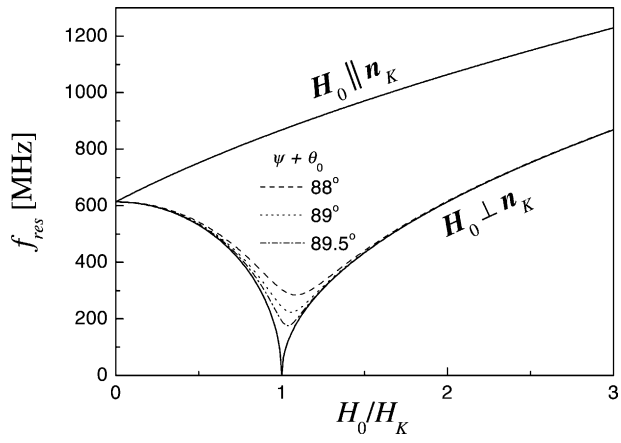

Fig. 4. Resonance frequencies of a single domain film with an in-plane.

The electromagnetic approximation was used for various model calculations. In case of strong skin effect (when the skin depth is much smaller than the transversal dimensions of the conductor) the skin layer can be approximated by a planar film and the surface impedance obtained for the film can be used for a conductor of any cross-section. In the case of weak skin effect, the solution of Eq. (3) is more complicated and sometimes only approximate solutions have been found. Cylindrical wires with different types of magnetic anisotropy were investigated in [12–14]. A composite wire consisting of a non-magnetic inner core and an axially magnetized outer shell with longitudinal anisotropy was described by Usov et al. [15]. Magnetoimpedance of a planar bi-layer film with crossed anisotropy, which is qualitatively similar to the wire with helical anisotropy, can be found in [16].

2.3.2. Exchange-conductivity models

The electromagnetic models, mentioned above, describe qualitatively well the basic features of GMI and can explain most of the experimental results. There are, however, some aspects, which cannot be explained in this frame and require more rigorous theoretical treatment, which takes into account the exchange stiffness. When the exchange term is included into the effective field $\boldsymbol{H}_\mathrm{eff}$ the Landau–Lifshitz and Maxwell equations cannot be separated and must be solved simultaneously. They provide a system of six partial differential equations for the vector components of $\boldsymbol{m}$ and $\boldsymbol{h}$. Their solutions must satisfy the boundary conditions, which combine the usual electromagnetic conditions with the surface spin-pinning. The general solution of Eqs. (3) and (4) consists of four pairs of wave modes, which besides the two pairs of electromagnetic modes, considered in the electromagnetic approximation, include also two pairs of spin waves [17]. As a consequence of hybridization of electromagnetic and spin-wave modes the exchange-conductivity effect appears, which can influence the GMI magnitude in the low and medium frequency regions.

The exchange-conductivity effect is caused by the inter-play between the skin effect and the exchange interaction. Because within the skin depth the ac component of magnetization $\boldsymbol{m}$ decreases from its surface value to zero in the bulk, the magnetization is inhomogeneous and exchange energy increases. Therefore, the exchange interaction weakens the skin effect and enhances the skin depth. In other words, the inhomogeneous ac field excites spin waves with wavelengths of the order of skin depth, which enhance the energy dissipation by eddy currents. It may be roughly interpreted as an apparent increase of resistivity in ferromagnetic metals.

The exchange-conductivity models of GMI are formally equivalent to the theory of ferromagnetic resonance in metals [9]. The main difference is that at FMR the samples are completely saturated, while in GMI experiment this

assumption need not be satisfied. This makes the theory of GMI more complicated. Also the low-signal condition, which is well satisfied in the low power FMR experiments, can be easily violated in the GMI measurements. Before describing the GMI models, let us first mention the basic outcomes of the FMR theory.

For a conductor with planar geometry, the general solution of Eqs. (3) and (4) is assumed in the form of a superposition of plane waves, $e^{-i\boldsymbol{kr}}$, propagating perpendicularly to the surface. For a general orientation of wave vector $\boldsymbol{k}$ with respect to $\boldsymbol{M}_0$ the secular equation for its magnitude is quartic in k^2, leading to four pairs of waves $-k_0$, k_0; $-k_1$, k_1; $-k_2$, k_2; $-k_3$, k_3 of mixed spin wave and electromagnetic character [18]. The amplitudes of individual waves are determined by the boundary conditions. In case of parallel resonance, which is usually realized in GMI experiments, $\boldsymbol{M}_0$ lies in the sample plane and consequently the waves propagate in the perpendicular direction. Then the secular biquartic equation decomposes into $k_0 = (1 - i)/\delta_0$, which corresponds to the non-magnetic skin effect for longitudinally polarized electromagnetic waves, and the bicubic equation:

$$k^6 + c_1k^4 + c_2k^2 + c_3 = 0 \tag{17}$$

for the three pairs of transversally polarized "magnetic" waves. At very high frequencies the electromagnetic and spin-wave branches can be well distinguished. But below certain, so called "cross-over", frequency the two wave branches become strongly mixed near the resonance [17]. It is just the region where the exchange-conductivity effect is observed. Procedures similar to the FMR theory were used to describe GMI in planar films and circular cylinders.

A single-domain planar film with an in-plane anisotropy (see Fig. 3) was investigated in [8]. It was shown that for an oblique magnetization ($\theta_0 \neq 0$) the impedance can be described by the two dimensional tensor $\hat{Z}$, which is diagonal in the coordinate system (x, y', z') related to the equilibrium direction $\boldsymbol{M}_0$. For an arbitrary direction of driving current I_{ac}, the impedance is:

$$Z = Z_{y'y'} \sin^2 \beta + Z_{zz} \cos^2 \beta \tag{18}$$

where β is the angle between magnetization $\boldsymbol{M}_0$ and the driving current. The transverse non-magnetic component $Z_{y'y'}$ of impedance tensor is given by Eq. (6) with $k = k_0$. An analytic formula for the longitudinal component Z_{zz} was obtained from the boundary conditions for free surface spins.

GMI in cylindrical wires was investigated by Ménard et al. [19,20]. An analytical expression for the surface impedance Z_s was found. When the anisotropy and exchange interaction were neglected, the formula for impedance reduced to Eq. (5) with k corresponding to the Larmor electromagnetic wave. For helical anisotropy, the surface impedance is:

$$Z_s = \frac{1 + Z_0Z_M + \sqrt{(1 - Z_0Z_M)^2 - (Z_0 - Z_M)^2 \sin^2 2\theta_0}}{2(Z_0 \cos^2 \theta_0 + Z_M \sin^2 \theta_0)} \tag{19}$$

where $Z_0 = \zeta_{y'y'}$ and $Z_M = \zeta_{z'z'}$ are the diagonal components of surface impedance tensor $\hat{\zeta}$. For $|Z_0|, |Z_M| \ll 1$, this formula reduces to an expression similar to Eq. (18). The solution of secular Eq. (17) and analytic formula for Z_M were simplified by neglecting the contribution of anti-Larmor spin wave. Using the simplified solution they have shown that, when the damping is neglected ($\alpha = 0$), the minimum skin depth is given by

$$\delta_{min} \approx \left(\frac{A\rho}{\omega\mu_0^2 M_s^2} \right)^{1/4} \tag{20}$$

for ω below the cross-over frequency:

$$\omega_c = \frac{4\alpha^2\gamma^2 A M_s}{\rho} \tag{21}$$

where the strong mixing of Larmor electromagnetic and spin-wave branches takes place. (A is the exchange stiffness constant.) In typical soft magnetic amorphous metals $\omega_c/2\pi$ is of the order 100 MHz. As a consequence of exchange-conductivity effect the maximum theoretical GMI ratio scales as $(\omega)^{1/4}$ at low and medium frequencies. Above ω_c the theoretical limit of GMI is given by Eq. (16).

3. Asymmetric GMI

Much attention has been paid recently to asymmetric GMI (AGMI) effect, which can be very promising for the development of auto-biased linear field sensors.

Asymmetric GMI was first announced by Kitoh et al. [21] for twisted Co-based amorphous wires with dc bias current superimposed on the driving current. Later on a similar effect was observed on as-quenched amorphous ribbons [22] and wires [23] and on Joule heated wires [24]. Field-annealing in air or moisture atmosphere with weak longitudinal or circumferential magnetic fields also produces AGMI in amorphous ribbons [25] and wires [26]. Gunji et al. [27] and Makhnovskiy et al. [28] reported another method of producing asymmetrical GMI characteristics, utilizing an axial ac-bias-field. Though the mechanisms of AGMI may be different and sometimes the origin of asymmetry is unknown, three different mechanism of AGMI can be now recognized:

- asymmetry due to dc bias current,
- asymmetry due to ac-bias-field,
- asymmetry due to exchange bias.

The principal features and the origins of these mechanisms are briefly discussed below.

3.1. AGMI due to dc bias current

This type of asymmetry is caused by the combination of helical magnetic anisotropy with circumferential dc

field produced by the bias current [21]. Similar asymmetry was observed on the as-quenched ribbons [22] and on as-quenched and Joule heated wires [23,24]. Even though the helical anisotropy was not intentionally induced in these cases the origin may be the same because it has been proved that in as-quenched wires some spontaneous helical anisotropy is present [29]. The same may be true for the as-quenched ribbons.

Without the bias current ($I_{dc} = 0$) a symmetric double-peak GMI curve is usually observed. When I_{dc} increases one peak enhances and the other diminishes, depending on I_{dc} orientation [22]. The positions of peaks, however, remain practically unchanged. When the direction of bias current is reversed the asymmetry also reverses. With increasing frequency, the asymmetry first increases and then decreases showing a maximum at a certain frequency. The asymmetry as a function of I_{dc}, measured at a constant frequency, also shows a maximum. For higher frequencies, the maximum shifts to higher currents, broadens and its height decreases [23].

The theoretical explanation, based on the electromagnetic model, was done by Panina and coworkers [14,30]. They showed that ζ_{zz} component of surface impedance becomes asymmetric, when a circumferential dc magnetic field H_ϕ is added. The asymmetry is related to the axial hysteresis loop, which is also asymmetric. The numerical simulations showed that for H_ϕ slightly higher then $H_K \sin\alpha$, where α is the angle between the circumferential and the easy directions (spiral angle), the hysteresis disappears and a large GMI asymmetry is observed.

A simple explanation of asymmetry can be obtained for the case of strong skin effect, when the skin layer can be approximated by a thin film on the wire surface. Using the resonance condition (15) with $\omega \to 0$ the approximate condition for maximum GMI can be obtained. The bias current I_{dc}, passing through the wire, produces the circumferential field $H_\phi = I_{dc}/2\pi a$ on the surface. Then the total dc field on the wire surface is $\sqrt{H_0^2 + H_\phi^2}$ and makes the angle $\arctan(H_\phi/H_0)$ with the axis. The resonance condition for the total dc field requires:

$$H_0 \approx H_K \cos\alpha \quad \text{and} \quad H_\phi \approx -H_K \sin\alpha \tag{22}$$

When the spiral angle of helical anisotropy is $\alpha \neq 0$, the resonance condition can be satisfied only for one orientation of H_0 and the asymmetry appears.

3.2. AGMI due to ac-bias-field

Gunji et al. [27] found AGMI in a CoFeSiB wire subjected to a pulse helical magnetic field, which was obtained by an ac pulse current passing through the wire and a coil wound around it (connected in series). The phenomenon was systematically investigated by Makhnovskiy et al. [28] on an as-quenched CoFeSiB wire using the driving current consisting of a harmonic current I_{ac} superimposed on a dc bias current I_{dc}. The circumferential and axial components of the helical field were provided by the wire and the magnetizing coil, respectively.

The asymmetry comes from the combination of helical magnetization with the axial ac field, which is described by the second term on the right hand side of Eq. (2). The first term on the right hand side is related to the circumferential magnetization process ($m_\phi - h_\phi$) and corresponds to the ordinary magnetoimpedance effect. The second term, on the other hand, corresponds to "cross-magnetization" process ($m_\phi - h_z$) [28], which is equivalent to Matteuchi effect [31]. If $\theta_0 \neq 0$ the off-diagonal element $\zeta_{z\phi}$ is non-zero and is an anti-symmetric function of H_0. The Matteuchi component of impedance can be controlled also by the ratio h_z/h_ϕ, i.e. by the number of turns of the driving coil. When this ratio is high only the Matteuchi effect contributes to the impedance and the asymmetry is the highest.

3.3. AGMI due to exchange bias

The third, and yet not well understood, type of AGMI was announced by Kim et al. [25]. A large asymmetry was observed in CoFeNiBSi ribbons field-annealed at 380 °C in air with a weak magnetic field H_a (4–240 A/m) along the ribbon. The samples annealed in vacuum did not show the asymmetry. The asymmetry in ribbons annealed in air depends on the magnitude and direction of H_a with respect to the measuring field H_0. For $H_a = 0$, a nearly symmetric double-peak GMI curve is observed. With increasing H_a, the peak for the same direction of H_0 increases and for the opposite direction decreases. A very large asymmetry is observed for $H_a > 40$ A/m at low frequencies (about 100 kHz) with a step-like change at $H_0 \approx 0$. This phenomenon is called the "GMI valve". The asymmetry decreases at higher frequencies, where the rotational contribution to GMI becomes dominant. Similar AGMI was reported for amorphous CoFeSiB wires field-annealed in a moist atmosphere with a weak circumferential field produced by dc current flowing though the wire [26]. A profound asymmetry was observed for the current above 4.5 mA.

The phenomenon was attributed to crystallization of the surface underlayer, which becomes to be depleted in B and Si due to the surface oxidation. This type of heat treatment is known to produce asymmetric hysteresis loops in amorphous ribbons due to the exchange interaction of amorphous bulk with the magnetically harder crystalline phase on the surface [32]. When the crystallization takes place in the presence of a weak magnetic field the crystallites are magnetically ordered, which results in an effective unidirectional surface anisotropy.

An attempt to explain the exchange-biased asymmetry theoretically by the quasistatic model, where the unidirectional exchange anisotropy was replaced by an effective dc-bias-field [33], was unsuccessful (see [34]). More theoretical work is needed to describe properly this phenomenon.

4. Materials optimization

The optimum GMI properties depend on the particular application, for which the GMI element should be used. For some applications also the fabrication simplicity and low cost are very important.

The most general requirements on GMI materials are the high GMI ratio and its sensitivity to applied magnetic field. Both these parameters require high magnetic softness. As can be seen from Eq. (16), the most important for the high theoretical GMI ratio are the high saturation magnetization, low resistivity and small ferromagnetic relaxation parameter α. While the rules for controlling the first two are sufficiently well known, there is only little known about the ferromagnetic relaxation. The gyromagnetic ratio γ is unimportant, because it changes only in the range of few percent for all 3d-based ferromagnetic metals. Because the relative change of impedance scales theoretically as H_0/H_K weak magnetic anisotropy is important for achieving high field sensitivity.

As has been shown, the theoretical skin depth can be hardly achieved at the driving frequencies below 1 GHz, where most of the practical applications are expected. There the another material parameters become more important. A good criterion for large GMI ratio at the intermediate frequencies, where the magnetization rotation dominates, is:

> How precisely the FMR resonance condition can be fulfilled in the whole volume of the skin layer?

From this point of view uniaxial magnetic anisotropy, perpendicular to the direction of internal dc field, is the best. There are few ways how to obtain anisotropy perpendicular to the axis of conductor:

- *Field-annealing*: In ribbons or films, it can be induced by annealing in transversal magnetic field. In wires, the circumferential magnetic field produced by applied current should be used.
- *Stress-annealing*: In Co-rich amorphous alloys (ribbons or wires), tensile stress along the conductor is applied during annealing.
- *Stress-induced anisotropy*: In materials with negative magnetostriction tensile stress induces the transversal anisotropy. In glass-covered microwires the glass coat itself produces this kind of stress.

Any fluctuations of local magnetic anisotropy (especially the orientation of easy axis) substantially deteriorate the GMI magnitude. Therefore, either the inhomogeneous internal stresses should be reduced as much as possible or materials with very low magnetostriction should be used.

The fluctuation of saturation magnetization can also lead to the spread of resonance field and the deterioration of GMI. It is not only because M_s directly appears in Eq. (15) but also because such fluctuations lead to random magnetostatic fields, which would appear in the total internal dc field $\boldsymbol{H}_0$.

Finally, the surface roughness should be mentioned. It is quite evident that for large skin effect the surface quality plays an important role. It is not only because the skin depth may become smaller than the surface irregularities, but also because of stray fields, which appear on the rough surface. The dc component of stray fields can cause the fluctuation of $\boldsymbol{H}_0$, as mentioned above. The ac component, on the other hand, caused the two-magnon scattering and increases the ferromagnetic relaxation. High quality surfaces can be obtained for glass-coated microwires or films prepared by vacuum or electro-deposition techniques.

In AGMI elements, which are required for linear field sensors, the asymmetry of GMI curve is an additional important parameter. Only two of the three AGMI types are useful for practical applications. The ac-bias-field AGMI can be left out. First, it is based on Matteuchi effect. Second, it brings only little improvement with respect to the classical dc-bias-field method, because additional magnetizing coils are required in both cases.

The asymmetry due to dc bias current can be controlled by the anisotropy field H_K, the spiral angle α and the bias current I_{dc}. To determine the optimum H_K and α more detailed theoretical analysis is required. The optimum bias current can be, however, estimated from the condition (22).

The exchange-biased AGMI, which does not require any bias current, is the most promising for practical applications. It is now restricted only to amorphous alloys and its deeper understanding requires further experimental and theoretical work.

Acknowledgements

Financial support of Project AVOZ-010-914 is appreciated.

References

[1] L.D. Landau, E.M. Lifshitz, Electrodynamics of Continuous Media, Pergamon Press, Oxford, 1975.
[2] K. Mohri, et al., IEEE Trans. Magn. MAG-28 (1992) 3150.
[3] F.L.A. Machado, S.M. Rezende, J. Appl. Phys. 79 (1996) 6558.
[4] D. Atkinson, P.T. Squire, J. Appl. Phys. 83 (1998) 6569.
[5] L.V. Panina, et al., IEEE Trans. Magn. 31 (1995) 1249.
[6] L.V. Panina, K. Mohri, Appl. Phys. Lett. 65 (1994) 1189.
[7] D.-X. Chen, J.L. Muñoz, A. Hernando, M. Vázquez, Phys. Rev. B 57 (1998) 10699.
[8] L. Kraus, J. Magn. Magn. Mater. 195 (1995) 764.
[9] A. Yelon, D. Ménard, M. Brittel, P. Ciureanu, Appl. Phys. Lett. 69 (1996) 3084.
[10] L. Kraus, J. Magn. Magn. Mater. 196–197 (1999) 354.
[11] D. Ménard, L.G.C. Melo, M.R. Brittel, P. Ciureanu, A. Yelon, M. Rouabhi, C.W. Cochrane, J. Appl. Phys. 87 (2000) 4801.
[12] N.A. Usov, A.S. Antonov, A.N. Lagar'kov, J. Magn. Magn. Mater. 185 (1998) 159.
[13] N.A. Usov, A.S. Antonov, A.N. Lagar'kov, A.B. Granovsky, J. Magn. Magn. Mater. 203 (1999) 108.
[14] D.P. Makhnovskiy, L.V. Panina, D.J. Mapps, Phys. Rev. B 63 (2001) 144424.

[15] A. Usov, A. Antonov, A. Granovsky, J. Magn. Magn. Mater. 171 (1997) 64.
[16] D.P. Makhnovskiy, A.S. Antonov, A.N. Lagar'kov, L.V. Panina, J. Appl. Phys. 84 (1998) 5698.
[17] C.E. Patton, Czech. J. Phys. B 26 (1976) 925.
[18] R.F. Sooho, Phys. Rev. 120 (1960) 1978.
[19] D. Ménard, M. Britel, P. Ciureanu, A. Yelon, J. Appl. Phys. 84 (1998) 2805.
[20] D. Ménard, A. Yelon, J. Appl. Phys. 88 (2000) 379.
[21] T. Kitoh, K. Mohri, T. Uchiyama, IEEE Trans. Magn. 31 (1995) 3137.
[22] F.L.A. Machado, A.R. Rodrigues, A.A. Puça, A.E.P. de Araújo, Mater. Sci. Forum 302–303 (1999) 202.
[23] S.H. Song, K.S. Kim, S.C. Yu, C.G. Kim, M. Vazquez, J. Magn. Magn. Mater. 215–216 (2000) 532.
[24] C. Gómez-Polo, M. Vazquez, M. Knobel, Appl. Phys. Lett. 78 (2001) 246.
[25] C.G. Kim, K.J. Jang, H.C. Kim, S.S. Yoon, J. Appl. Phys. 85 (1999) 5447.
[26] S.H. Song, S.C. Yu, C.G. Kim, H.C. Kim, W.Y. Lim, J. Appl. Phys. 87 (2000) 5266.
[27] T. Gunji, L.V. Panina, K. Mohri, J. Magn. Soc. Jpn. 21 (1997) 793 (in Japanese).
[28] D.P. Makhnovskiy, L.V. Panina, D.J. Mapps, Appl. Phys. Lett. 77 (2000) 121.
[29] J.M. Blanco, A. Zhukov, A.P. Chen, A.F. Cobeno, A. Chizhik, J. Gonzalez, J. Phys. D Appl. Phys. 34 (2001) L31.
[30] L.V. Panina, K. Mohri, D.P. Makhnovskiy, J. Appl. Phys. 85 (1999) 5444.
[31] L. Kraus, S.N. Kane, M. Vázquez, G. Rivero, E. Fraga, A. Hernando, J.M. Barandiarán, J. Appl. Phys. 75 (1994) 6952.
[32] K.H. Shin, C.D. Graham Jr., P.Y. Zhou, IEEE Trans. Magn. 28 (1992) 2772.
[33] C.G. Kim, K.J. Jang, D.Y. Kim, S.S. Yoon, Appl. Phys. Lett. 75 (1999) 2114.
[34] D.-X. Chen, L. Pascual, A. Hernando, Appl. Phys. Lett. 77 (2000) 1727.